

Aerosol optical properties in the North China Plain

N. Ma et al.

Aerosol optical properties in the North China Plain during HaChi campaign: an in-situ optical closure study

N. Ma¹, C. S. Zhao¹, A. Nowak², T. Müller², S. Pfeifer², Y. F. Cheng³, Z. Z. Deng¹, P. F. Liu¹, W. Y. Xu¹, L. Ran¹, P. Yan⁴, T. Göbel², E. Hallbauer², K. Mildenerberger², S. Henning², J. Yu⁵, L. L. Cheng⁵, X. J. Zhou^{1,4}, F. Stratmann², and A. Wiedensohler²

¹Department of Atmosphere, School of Physics, Peking University, Beijing, China

²Leibniz Institute for Tropospheric research, Leipzig, Germany

³Center of Global and Regional Environment Research, University of Iowa, Iowa, USA

⁴Chinese Academy of Meteorological Sciences of CMA, Beijing, China

⁵Wuqing Meteorological Bureau of Tianjin, Tianjin, China

Received: 8 March 2011 – Accepted: 15 March 2011 – Published: 22 March 2011

Correspondence to: C. S. Zhao (zcs@pku.edu.cn)

Published by Copernicus Publications on behalf of the European Geosciences Union.

Title Page

Abstract Introduction

Conclusions References

Tables Figures

◀ ▶

◀ ▶

Back Close

Full Screen / Esc

Printer-friendly Version

Interactive Discussion



Abstract

The largest uncertainty in the estimation of radiative forcings on climate stems from atmospheric aerosols. In winter and summer of 2009, two periods of in-situ measurements on aerosol physical and chemical properties were conducted within the HaChi project at Wuqing, a town between Beijing and Tianjin in the North China Plain (NCP). Aerosol optical properties including scattering coefficient (σ_{sp}), hemispheric back scattering coefficient (σ_{bsp}), absorption coefficient (σ_{ap}), as well as single scattering albedo (ω) are presented. The characteristics of diurnal and seasonal variations are analyzed together with the meteorological and satellite data. The mean values of $\sigma_{\text{sp},550\text{ nm}}$ of the dry aerosol in winter and summer are 280 ± 253 and $379 \pm 251 \text{ Mm}^{-1}$, respectively. The average σ_{ap} for the two periods are respectively 47 ± 38 and $43 \pm 27 \text{ Mm}^{-1}$. The mean values of ω are 0.83 ± 0.05 and 0.87 ± 0.05 for winter and summer, respectively. The relative high levels of σ_{sp} and σ_{bsp} are representative of the regional polluted aerosol of the North China Plain. Pronounced diurnal cycle of σ_{sp} , σ_{ap} and ω are found, mainly influenced by the evolution of boundary layer and accumulation of local emissions during night-time. Regional transport of pollutants from southwest in the NCP is significant both in winter and summer, while high values of σ_{sp} and σ_{ap} correlate with calm winds in winter, which indicating the significant contribution of local emissions. An optical closure experiment is conducted to better understand uncertainties of the measurements. Good correlations ($R > 0.98$) are found between values measured by nephelometer and values calculated with a modified Mie model. Monte Carlo simulations show an uncertainty of about 30% for the calculations. Considering all possible uncertainties of measurements, calculated σ_{sp} and σ_{bsp} agree well with measured values, indicating a stable performance of instruments and thus a reliable aerosol optical data.

Aerosol optical properties in the North China Plain

N. Ma et al.

[Title Page](#)[Abstract](#)[Introduction](#)[Conclusions](#)[References](#)[Tables](#)[Figures](#)[◀](#)[▶](#)[◀](#)[▶](#)[Back](#)[Close](#)[Full Screen / Esc](#)[Printer-friendly Version](#)[Interactive Discussion](#)

1 Introduction

Atmospheric aerosols influence the earth's radiation budget directly by scattering and absorbing solar radiation (Charlson et al., 1992), and indirectly by acting as condensation nuclei in cloud formation, thus affecting the optical properties and lifetimes of clouds (Twomey, 1974; Albrecht, 1989; Rosenfeld, 1999, 2000). The radiative forcing of these two effects is estimated at -0.5 Wm^{-2} and -0.7 Wm^{-2} , respectively, with the largest uncertainty of $+0.8/-1.5 \text{ Wm}^{-2}$ among all climate forcing factors (IPCC, 2007). One of the reasons for such great uncertainties is that aerosols have highly inhomogeneous horizontal and vertical distributions (van Donkelaar et al., 2010; Liu et al., 2009) as well as temporal variations, different from well mixed greenhouse gases, such as CO_2 and methane. To better understand the direct effect of aerosols, further knowledge of aerosol optical properties is of critical importance. The aerosol optical properties, e.g., scattering coefficient (σ_{sp}), absorption coefficient (σ_{ap}), aerosol optical depth (AOD) and single scattering albedo (ω), are closely related to the aerosol physical and chemical characteristics, which are influenced by many processes, such as aerosol formation, growth and removal. To estimate the aerosol optical properties and radiative impacts with the measured physical and chemical characteristics, Mie model and radiative transfer models are widely employed. However, due to the uncertainties in measurements and models, the calculations are needed to be evaluated (Seinfeld and Pandis, 1998; Quinn et al., 1998; Bond et al., 1998; Sheridan et al., 2001). Therefore, more investigations on aerosol optical properties and optical closure studies are urgently needed especially in regions such as Asia, Africa, and South-America.

Closure studies are usually used for estimating the uncertainties of different measurement techniques and numerical models. Quinn et al. (1996) reviewed some of these closure studies in the research of aerosols. A typical closure study requires an over-determined set of observations. Then a comparison between a measured value of an important system property and a value calculated with an appropriate model based on independent measurements can be made. Closure is achieved if there is an

Aerosol optical properties in the North China Plain

N. Ma et al.

Title Page

Abstract

Introduction

Conclusions

References

Tables

Figures

◀

▶

◀

▶

Back

Close

Full Screen / Esc

Printer-friendly Version

Interactive Discussion



agreement between these two values within the accepted level of uncertainty (Quinn et al., 1998). Closure study can be used as an examination of the measurements and models. It also provides a platform for sensitivity studies as well as an approach to evaluate and reduce the uncertainties of both measurements and models. Some optical closure studies were already done in the past decades (e.g. Wex et al., 2002a; Cheng et al., 2007, 2009; Pesava et al., 2001).

Along with the rapid growth of population and economy in China, emissions of anthropogenic pollutants increased dramatically in the past several decades. Urbanization and industrial activities produce large amounts of aerosols, especially in the North China Plain (NCP). Aerosol optical properties in China are highly complex and differ from those in Europe or North America (Holler et al., 2003). Moreover, the widespread consumptions of coal and biomass fuels make China a significant source region of black carbon (BC). It was reported that the BC amount emitted in China was around one fourth of global anthropogenic BC emissions (Cooke et al., 1999; Street et al., 2001; Bond et al., 2004). In the past decade, there were some studies focusing on aerosol optical properties (Yan et al., 2008; Xu et al., 2002, 2004; Cheng, 2008a, 2009), but only a few studies touched the uncertainty evaluation of measured aerosol properties and related models (Cheng et al., 2007).

In this paper, the results of aerosol optical property observations during a two-period in-situ measurement campaign at a site in the north of NCP are presented, the characteristics of aerosol optical properties are analyzed. An aerosol optical closure study between measured and calculated aerosol scattering coefficient and related uncertainty evaluation is shown.

Aerosol optical properties in the North China Plain

N. Ma et al.

Title Page

Abstract

Introduction

Conclusions

References

Tables

Figures

⏪

⏩

◀

▶

Back

Close

Full Screen / Esc

Printer-friendly Version

Interactive Discussion



2 Measurements

2.1 The field site

The data used in this study were collected during the HaChi (Haze in China) campaigns. Measurements of aerosol optical, chemical, hygroscopic properties and size distribution, as well as trace gases observations, were conducted in Wuqing in the north NCP in two periods of 2009: the winter campaign was from 6 March to 5 April (65–95 DOY); while the summer campaign from 12 July to 14 August (193–226 DOY).

The map of the NCP is shown in Fig. 1. The population is dense and the land use is mainly agriculturally in the NCP. Several big cities with rapid developing of economy and industry are located in the NCP. Wuqing (marked as a star in Fig. 1) is a town with about 0.8 million inhabitants, located between two megacities: Beijing (16 million inhabitants, 80 km away from Wuqing) and Tianjin (10 million inhabitants, 30 km away from Wuqing), in the north of the NCP. The site is located in the suburban area in Wuqing and thus representative for the anthropogenic regional aerosol.

An automatic weather station (AWS) is located next to the aerosol measurement containers. During the whole campaign, meteorological parameters, such as wind speed, wind direction, relative humidity (RH) and temperature (T) were measured continuously and reported as 1-min data. The weather conditions were either clear or cloudy during the winter campaign, and no precipitation events occurred; while there were 10 rain events in the summer campaign. In both of the two periods, the wind direction is dominated of southwest, with average wind speeds of $3.2 \pm 2.2 \text{ m s}^{-1}$ and $1.8 \pm 1.2 \text{ m s}^{-1}$, respectively. T and RH show an evident diurnal cycles (Fig. 2). Average T and RH are $7.8 \pm 5.6 \text{ }^\circ\text{C}$ and $42.2 \pm 20.7\%$ in winter, $26.3 \pm 3.4 \text{ }^\circ\text{C}$ and $75.4 \pm 15.3\%$ in summer, respectively.

Most of the ground-based measurements were conducted in a measurement container, in which the temperature was maintained at $22 \text{ }^\circ\text{C}$. The sample air was collected with a PM_{10} inlet (16.67 L min^{-1}) installed on the top of a stainless steel tube with a diameter of $3/4$ inch and 7 m above the ground level. The sample air was split into

Aerosol optical properties in the North China Plain

N. Ma et al.

Title Page

Abstract

Introduction

Conclusions

References

Tables

Figures

◀

▶

◀

▶

Back

Close

Full Screen / Esc

Printer-friendly Version

Interactive Discussion



several flows inside the container, passing through stainless steel tubing, to different instruments. The residence time for the sample air in the inlet line was about 5 s. An automatic aerosol diffusion dryer (Tuch et al., 2009) was set upstream all of the instruments, to keep the RH of the sample air below 30%.

2.2 Nephelometer measurements

The σ_{sp} and σ_{bsp} for dry aerosols were measured by a total/back integrating nephelometer at wavelengths of 450, 550 and 700 nm (TSI, Inc., Shoreview, MN USA, Model 3563) (Heintzenberg and Charlson, 1996; Anderson et al., 1996, 1998). The temporal resolution of measurement was 1 min. However, in this study, 10-min averaged data was used. The Nephelometer was calibrated before each of the two campaigns using CO_2 (Anderson et al., 1996). Particle free air checks were performed once a day. The truncation and non-Lambertian error was corrected using the modified Mie model, which applied in the closure study. The correction factor is defined as:

$$C = \frac{\sigma_{\text{sp,Mie}}}{\sigma_{\text{sp,Modified-Mie}}} \quad (1)$$

Where $\sigma_{\text{sp,Mie}}$ is the ideal scattering coefficient of dry aerosol calculated with a Mie theory, while $\sigma_{\text{sp,Modified-Mie}}$ is calculated with a Modified Mie model simulating the Nephelometer. The calculations are based on measured particle number size distribution (PNSD) and the black carbon (BC) concentration. The details will be described in Sect. 3.

2.3 MAAP measurements

A Multi-angle Absorption Photometer (MAAP Model 5012, Thermo, Inc., Waltham, MA USA) was employed to determine the σ_{ap} for dry particles. The instrument determines σ_{ap} via the simultaneous measurement of light (637 nm) passing through its filter and scattered back from particles accumulated on it. It operates at two detection angles to

Title Page

Abstract

Introduction

Conclusions

References

Tables

Figures

◀

▶

◀

▶

Back

Close

Full Screen / Esc

Printer-friendly Version

Interactive Discussion



resolve the influence of light-scattering aerosol components on the angular distribution of the back-scattered radiation (Petzold and Schönlinner, 2004). The MAAP provides the BC mass concentrations in the unit of $\mu\text{g m}^{-3}$. According to the manual, σ_{ap} at 637 nm can be calculated with $\sigma_{\text{ap}} = \rho_{\text{BC}} \cdot 6.6 \text{ m}^2 \text{ g}^{-1}$, where ρ_{BC} is the mass concentration of BC. The sampling frequency was 1 min, and 10-min averaged data was used.

2.4 TDMPS/APS measurements

A Tandem Differential Mobility Particle Sizer (TDMPS, IfT, Leipzig, Germany) (Birmili et al., 1999) was used to measure aerosol PNSD with electrical mobility diameter from 3 to 800 nm. An Aerodynamic Particle Sizer (APS Model 3320, TSI, Inc., Shoreview, MN USA) was employed to measure aerosol PNSD with aerodynamic diameters from 0.5 to 10 μm . Both of them were operated under dry conditions. It took 10 min for a complete scan for both TDMPS and APS. A series of processing was applied to the TDMPS data. Following the procedure described by Wiedensohler et al. (1997), the counting efficiencies of CPC (TSI 3010) and UCPC (TSI 3025) were measured beforehand. Inversion of the raw data was done according to an algorithm introduced by Stratmann and Wiedensohler (1996). Electrical mobility diameters measured by TDMPS and aerodynamic diameters measured by APS were converted to volume equivalent diameter (DeCarlo et al., 2004). Then aerosol PNSD measured by TDMPS and APS was combined to yield aerosol size distributions with diameter range from 3 nm to 10 μm . Furthermore, the PNSD data was corrected for diffusion losses, gravitational losses and impaction losses in the sampling tubes.

3 Methods of optical closure for dry aerosol

An optical closure for dry aerosols is carried out to better understand the dependence of aerosol optical properties on their physical and chemical characterizations, and to evaluate the quality of the measurements.

Aerosol optical properties in the North China Plain

N. Ma et al.

Title Page

Abstract

Introduction

Conclusions

References

Tables

Figures

◀

▶

◀

▶

Back

Close

Full Screen / Esc

Printer-friendly Version

Interactive Discussion



Aerosol optical properties in the North China Plain

N. Ma et al.

Title Page

Abstract

Introduction

Conclusions

References

Tables

Figures

◀

▶

◀

▶

Back

Close

Full Screen / Esc

Printer-friendly Version

Interactive Discussion



A two-component optical aerosol model (Wex et al., 2002a; Cheng et al., 2006) is used for dry aerosol optical closure. In this model, aerosol species are divided into light-absorbing BC and non-light-absorbing components such as sulfate, nitrate, ammonium, OC and other undetermined ones, since σ_{sp} is not sensitive to the mass fraction of these non-light-absorbing components (Wex, 2002b).

To obtain the size-resolved volume fraction of BC, the BC mass size distribution observed in CAREBeijing (Cheng et al., 2009) was used in this study. In Cheng's work, size-resolved BC mixing states was measured by a Volatility Tandem Differential Mobility Analyser (VTDMA) at the regional site Yufa south of Beijing during the summer of 2006. Both of Yufa and Wuqing are located in the Mega city cluster of Beijing and Tianjin. The two sites, about 60 km away from each other, have similar surroundings and pollution levels. Both of them are located in suburban areas and are influenced mainly by the regional pollution transported from southern industrialized regions. Thus, the BC mass size distribution normalized by the total mass concentration in Wuqing is assumed to be the same as the average one in Yufa. The BC mass concentration at a given particle size and time can be calculated as the following equation:

$$m(\log D_p, t)_{Wuqing, BC} = \frac{m(\log D_p)_{Yufa, external, ave} + m(\log D_p)_{Yufa, internal, ave}}{\sum_{\log D_p} (m(\log D_p)_{Yufa, external, ave} + m(\log D_p)_{Yufa, internal, ave})} \cdot m(t)_{MAAP, Wuqing} \quad (2)$$

where, $m(\log D_p)_{Yufa, external, ave}$ represents the average mass concentration of externally mixed BC in size bin D_p measured at Yufa, while $m(\log D_p)_{Yufa, internal, ave}$ is the average mass concentration of internally mixed BC at D_p . $m(t)_{MAAP, Wuqing}$ is the total mass concentration of BC measured by MAAP at Wuqing.

In other words, only the normalized BC mass size distribution measured at Yufa was used here. The BC mass concentration was kept to be same as the values derived from the MAAP measurements at Wuqing. The BC volume fraction at each size is calculated as:

$$f(\log D_p)_{BC,V} = \frac{m(\log D_p, t)_{BC}}{\rho_{BC} \cdot V(\log D_p, t)_{TDMPS\&APS}} \quad (3)$$

where, $V(\log D_p, t)_{TDMPS\&APS}$ is the volume concentration of sampled aerosol in size bin D_p measured by TDMPS or APS, and ρ_{BC} is the density of BC.

In literature (Sloane et al., 1983, 1984, 1991; Sloane and Wolff, 1985; Ouimette and Flagan, 1982; Seinfeld and Pandis, 1998), the density of BC is reported as a range from 1.00 g cm^{-3} to 2.00 g cm^{-3} . Accordingly, an average value of 1.5 g cm^{-3} is used, and the uncertainty (3σ) is assigned to be 33% covering the possible range.

Lacking of measurements of BC mixing state, completely external mixture and internal mixture of BC is assumed for the two-component optical aerosol model. Because atmospheric aerosols are probably partial combination of internally and externally mixed particles (Wex, 2002a; Chandra et al., 2004), the $\sigma_{sp}(\sigma_{bsp})$ measured by Nephelometer should be within the range determined by the calculated values based on the assumption of external mixture and internal mixture of BC.

For the case of completely external mixture, the PNSD of BC and non-absorbing component are obtained by multiplying the aerosol PNSD with $f(\log D_p)_{BC,V}$ and $1 - f(\log D_p)_{BC,V}$, respectively. The refractive index used for BC component is $\tilde{m}_{BC} = 1.96 - 0.66i$ (Seinfeld and Pandis, 1998), and for non-absorbing component it is set to $\tilde{m}_{non} = 1.53 - 10^{-7}i$ (Wex et al., 2002a).

For completely internal mixture aerosol, the BC is considered to be homogeneously mixed with non-absorbing component with the size dependent volume fraction $f(\log D_p)_{BC,V}$. The refractive index is derived as a volume-weighted average between the two components:

$$\tilde{m}(\log D_p) = f(\log D_p)_{BC,V} \tilde{m}_{BC} + (1 - f(\log D_p)_{BC,V}) \tilde{m}_{non} \quad (4)$$

The refractive indices \tilde{m} is size dependent, due to the size dependence of $f(\log D_p)_{BC,V}$. Based on Mie theory (Mie, 1908), the scattering efficiency Q_{sp} and hemispheric back

Aerosol optical properties in the North China Plain

N. Ma et al.

Title Page

Abstract

Introduction

Conclusions

References

Tables

Figures

◀

▶

◀

▶

Back

Close

Full Screen / Esc

Printer-friendly Version

Interactive Discussion



scattering efficiency Q_{bsp} can be calculated by integrating the scattering intensity function $|S(\theta, x, \tilde{m})|$ from 0° to 180° and from 90° to 180° , respectively:

$$Q_{\text{sp,bsp}} = \frac{1}{x^2} \int_{\theta} |S(\theta, x, \tilde{m})|^2 \sin\theta d\theta \quad (5)$$

where, $x = \pi D_p / \lambda$. D_p is the volume equivalent diameter of particles. λ is the wavelength of light, and θ is the scattering angle.

Different from the scattering angle ranges in Mie theory, the scattering integration angle of TSI 3563 integrating nephelometer is from 7° to 170° for scattering and from 90° to 170° for hemispheric back scattering, respectively. Thus, the measured values are truncated in the near-forward and near-backward angular ranges. Furthermore, the light source of nephelometer is not strictly Lambertian and shows a non-ideal angular response (Anderson et al., 1996). These two factors account for the main systematic errors of nephelometer measurements and these two effects must be corrected.

The angular response is solved in the Mie calculations based on the Bohren-Huffman Mie model (BHMIE) (Bohren and Huffman, 1983). The $\sin\theta$ term in Eq. (5) is replaced by the angular sensitivity curves $f(\theta)_{\text{sp}}$ and $f(\theta)_{\text{bsp}}$, derived from a calibration experiment of the TSI 3563 nephelometer (Anderson et al., 1996). The σ_{sp} and σ_{bsp} are calculated as:

$$\sigma_{\text{sp,bsp}} = \int_{D_p} \left[\frac{1}{x^2} \int_{\theta} |S(\theta, x, \tilde{m})|^2 f(\theta)_{\text{sp,bsp}} d\theta \right] \cdot \left(\frac{\pi}{4} D_p^2 \right) \cdot N(\log D_p) \cdot d \log D_p \quad (6)$$

where, $N(\log D_p)$ is the aerosol PNSD.

The modified Mie model introduced above, which simulate the measurements of TSI 3563 nephelometer, is applied in the correction for data of nephelometer measurements and the optical closure for dry particles. Comparison between calculated σ_{sp} (σ_{bsp}) and the values measured by Nephelometer is shown in Sect. 4.2.

Aerosol optical properties in the North China Plain

N. Ma et al.

Title Page

Abstract

Introduction

Conclusions

References

Tables

Figures

◀

▶

◀

▶

Back

Close

Full Screen / Esc

Printer-friendly Version

Interactive Discussion



Discussion Paper | Discussion Paper | Discussion Paper | Discussion Paper

4 Results and discussion

4.1 Measurements of aerosol optical properties

4.1.1 Overview

Table 1 summarizes the statistics on measured aerosol optical properties during the two campaigns. For 550nm, the mean σ_{sp} for the winter campaign and the summer campaign are 280 ± 253 and $379 \pm 251 \text{ Mm}^{-1}$, respectively. The mean σ_{ap} of the two campaigns are 47 ± 38 and $43 \pm 27 \text{ Mm}^{-1}$, respectively.

The σ_{sp} in Wuqing is lower than the mean value of Beijing ($488 \pm 370 \text{ Mm}^{-1}$) in June, 1999, while the σ_{ap} is half of that in Beijing ($83 \pm 40 \text{ Mm}^{-1}$) (Bergin et al., 2001). During January 2005, the σ_{sp} and σ_{ap} in Beijing had been found to be at an even higher level of 777 ± 689 and $89 \pm 74 \text{ Mm}^{-1}$, respectively (Heintzenberg et al., 2008).

Compared with regional sites around Beijing, the σ_{sp} and σ_{ap} in Wuqing are about a factor of 2 higher than the mean values measured in SDZ (175 ± 189 and $18 \pm 13 \text{ Mm}^{-1}$) during 2003 to 2005 (Yan et al., 2008). Garland et al. (2009) reported a mean σ_{sp} of $361 \pm 295 \text{ Mm}^{-1}$ and a mean σ_{ap} of $52 \pm 37 \text{ Mm}^{-1}$ measured in Yufa in summer of 2006. They are very similar to the values observed in Wuqing.

Compared with other regional sites in China, the σ_{sp} in Wuqing is similar to that in Lin'an ($353 \pm 202 \text{ Mm}^{-1}$) in November 1999 (Xu et al., 2002) and in Xinken, ($333 \pm 137 \text{ Mm}^{-1}$) in October 2004 (Cheng et al., 2008a). The σ_{ap} in Wuqing is a factor of 0.6 lower than that in Xinken ($70 \pm 42 \text{ Mm}^{-1}$), while it is double of that measured in Lin'an ($23 \pm 14 \text{ Mm}^{-1}$). Overall, σ_{sp} and σ_{ap} in Wuqing are higher than that in the rural area, while are lower than that measured in mega cities.

For seasonal comparison, the average σ_{sp} and σ_{bsp} are higher in summer than that in winter, while the average σ_{ap} shows an opposite variation. This is mainly due to the seasonal changes of air pollutants transportation. The changing of local pollutant emissions is also one of the potential players. Details will be discussed in Sects. 4.1.2 and 4.1.3.

Aerosol optical properties in the North China Plain

N. Ma et al.

Title Page

Abstract

Introduction

Conclusions

References

Tables

Figures

◀

▶

◀

▶

Back

Close

Full Screen / Esc

Printer-friendly Version

Interactive Discussion



Aerosol optical properties in the North China Plain

N. Ma et al.

Title Page

Abstract

Introduction

Conclusions

References

Tables

Figures

◀

▶

◀

▶

Back

Close

Full Screen / Esc

Printer-friendly Version

Interactive Discussion



The single scattering albedo, defined as $\omega = \sigma_{\text{sp}} / (\sigma_{\text{sp}} + \sigma_{\text{ap}})$, is one of the most important parameters in estimating of the direct aerosol radiative forcing. Even a small error in its estimation might change the sign of aerosol radiative forcing (Takemura et al., 2002). To calculate ω , a wavelength correction for aerosol absorption is applied to the measured σ_{ap} using an empirical approach, $\sigma_{\text{ap}} \propto \lambda^\beta$, with the absorption exponent $\beta = 1$ (wavelength λ in the interval 0.45–0.70 μm) (Bodhaine, 1995).

The average ω at the wavelength of 550 nm in Wuqing is 0.83 ± 0.05 in winter and 0.87 ± 0.05 in summer, respectively. These values are similar as that measured in Yufa, which is 0.86 ± 0.07 at wavelength of 532 nm (Garland et al., 2009). Yan et al. (2008) reported a higher ω in winter (0.91 ± 0.03) and a lower ω in summer (0.86 ± 0.06) in SDZ. The ω in Wuqing is relatively low compared to the values retrieved through AERONET for the Northern Hemisphere (0.85–0.95) (Dubovik et al., 2002). Since our measurements are controlled at a RH below 30%. At ambient condition, water uptakes of aerosol would result in higher ω (Cheng et al., 2008b).

The average ω in winter is lower than that in summer, caused by higher emissions of BC in winter than that in summer (Zhang et al., 2009; Lu et al., 2010). In northern China, house heating in winter is provided by central heating plants, mainly fueled by coal. Aerosols with a relative high fraction of soot from combustion processes are emitted into the atmosphere.

4.1.2 Wind dependence of aerosol optical properties

Fig. 3 presents the wind dependence of the σ_{sp} , σ_{ap} and ω . From the wind rose (solid line), it can be found that the prevailing winds came from SSW for both winter and summer campaign. In winter, weather systems with strong winds in NNW direction occurred occasionally.

The average MODIS AOD distribution at the NCP during the two campaign periods is presented in Fig. 1. The AOD, which represents the columnar optical property of the aerosols at ambient condition, is influenced by many factors such as the vertical profiles of RH and PNSD. However, it can provide information about the distribution of

regional aerosol pollution, which can help to understand the wind dependence pattern of aerosol optical properties.

In both winter and summer, the average σ_{sp} and σ_{ap} (dash-dot line) for south winds (90° – 270°) are higher than that for north winds, caused by the transportation of pollutants from south areas. This can be seen through the AOD distribution in Fig. 1. In both winter and summer, the AOD of the south areas is obviously higher than that of the north areas. Since in the NCP, the major cities and industrial areas with high pollution emissions are mainly located in the southern region.

In winter, the maximum σ_{sp} and σ_{ap} occur with calm winds, independent on wind directions. This indicates that aerosol emissions of local sources mostly contribute to the aerosol pollution. It should be noticed that the average AOD in Beijing is higher than the area around. But the NW wind, which is at the direction of Beijing, does not cause high σ_{sp} and σ_{ap} . The reason is that in winter the NW winds usually occur with cold front system and with high wind speed. The dilution effect of such strong winds is more significant, and the strong north winds sweep away air pollutants, resulting in the low σ_{sp} and σ_{ap} in winter.

In summer, the maximum σ_{sp} and σ_{ap} occur with southerly winds, relating to the pollutants transportation from the southern region in the NCP, as shown in Fig. 1.

The wind maps of ω are shown in Fig. 3c and f. In both winter and summer, ω accompanied by calm winds are always lower than that under strong winds, indicating that the locally emitted aerosol contains a higher fraction of BC than the aerosols transported from surrounding areas. During the pollutants transporting, the aging process and secondary aerosol formation produce non-light-absorbing components. As indicated in Cheng et al. (2009), for aged aerosols, even though the coating effect increase the light absorbing of BC, the scattering increased by the secondary particles and condensations will still overcome the increases of the light absorbing, which resulting an increase of ω . The average ω for southerly winds is lower than that for northerly winds, which may relate to the denser industrialization in the south of the NCP.

Aerosol optical properties in the North China Plain

N. Ma et al.

Title Page

Abstract

Introduction

Conclusions

References

Tables

Figures

◀

▶

◀

▶

Back

Close

Full Screen / Esc

Printer-friendly Version

Interactive Discussion



4.1.3 Diurnal variation of aerosol optical properties

Figure 4 shows the average diurnal cycle of the wind speed, σ_{sp} , σ_{ap} and ω during the winter and summer campaign. Evident diurnal variations can be found for all of those variables, mainly determined by the diurnal cycle of the boundary layer height and the local emission pattern. The diurnal cycle of wind speed and secondary aerosol production are also potential players.

The diurnal pattern of the σ_{sp} and σ_{ap} are similar in winter and summer. The maximum of the σ_{sp} and σ_{ap} appear in the morning between 06:00 and 08:00. During this period, the rapid increase of the aerosol pollutants is mainly due to the morning traffic, just before the increase of the boundary layer height. The dilution effect of the increasing boundary layer height results in a decrease of the σ_{sp} and σ_{ap} between 08:00 and 14:00. They reach their minimum around 16:00. During night, the σ_{sp} and σ_{ap} remain at relative high values, since particle emissions are accumulated in the shallow nocturnal boundary layer.

The σ_{sp} and σ_{ap} are lower in winter than in summer during night. These differences are mainly caused by different levels of wind speed between winter and summer at night. The diurnal pattern of wind speed is shown in Fig. 4. Wind speed during night time in winter (approximately 3 m s^{-1}) is higher than that in summer (around 1.5 m s^{-1}). The higher wind speed in wintertime suppresses an increased accumulation at ground at night.

The ω diurnal pattern shows two dips in the morning and evening probably caused by the emission of diesel engine trucks, since trucks are forbidden to enter the city area of Wuqing during the daytime of 08:00–20:00. The maximum ω appears around 14:00. During daytime, the light-scattering aerosol is highly enhanced by secondary aerosol formation and aging processes, which rapidly occur in the NCP (Wu et al., 2007; Wiedensohler et al., 2009). This could be the potential explanation for the maximum ω in the afternoon.

Title Page

Abstract

Introduction

Conclusions

References

Tables

Figures

◀

▶

◀

▶

Back

Close

Full Screen / Esc

Printer-friendly Version

Interactive Discussion



The median values (dash) of all aerosol optical properties are typically different from mean values (dot), since the probability distributions of these variables are deviate from normal distribution. For σ_{sp} and σ_{ap} , the median values are lower than the arithmetic mean value, especially in winter campaign, indicating heavier pollution events in winter than in summer.

4.1.4 Aerosol optical properties in pollution episodes

Time series of measured optical properties for the PM_{10} aerosol at dry condition ($RH < 30\%$) are presented in Fig. 5. In both winter and summer, large temporal variations were found for all optical properties mainly relating to the changing of weather systems. Some heavy pollution events could be identified. A pollution episode is defined as a significant rise in σ_{sp} and σ_{ap} , satisfying that both of σ_{sp} and σ_{ap} are within the top 20% highest values with lasting time of at least 12 h. We determined three episodes in the winter and two in summer campaign, respectively, as shown in Fig. 5.

For the episodes in winter, the average $\sigma_{sp,550nm}$ and σ_{ap} are $742 \pm 283 Mm^{-1}$ and $112 \pm 37 Mm^{-1}$, respectively, which are about two times higher than the average value for the whole campaign. The average ω is 0.85 ± 0.03 , 2.4% higher than that of whole period. The prevailing winds during these the episodes are mainly from SSW and ESE, basically same as the prevailing winds for the whole period. Because of no NW wind of high speed, the average wind speed for the episodes (1.74 ± 1.17) is much less than that for the whole period (3.22 ± 2.18). It seems that these episodes in winter occur in stable weather systems. The accumulation of locally emitted aerosol particles causes relative high σ_{sp} and σ_{ap} , and aging process causes high ω (Cheng et al., 2009).

For the episodes in summer, the average $\sigma_{sp,550nm}$ and σ_{ap} are $874 \pm 282 Mm^{-1}$ and $85 \pm 26 Mm^{-1}$, respectively. The average ω is 0.9 ± 0.03 , 3.5% higher than that of whole period. The winds directions during these episodes are from S and SSW, with the average wind speed of 1.78 ± 0.57 , close to the average value of the whole period (1.84 ± 1.17). The episodes in summer are all caused by the transportation of air pollutants from the southern regions under the consecutive south winds.

Aerosol optical properties in the North China Plain

N. Ma et al.

[Title Page](#)[Abstract](#)[Introduction](#)[Conclusions](#)[References](#)[Tables](#)[Figures](#)[⏪](#)[⏩](#)[◀](#)[▶](#)[Back](#)[Close](#)[Full Screen / Esc](#)[Printer-friendly Version](#)[Interactive Discussion](#)

4.2 Optical closure for dry particles

4.2.1 Comparison of measured and calculated optical properties for dry particles

For the optical closure of the dry PM_{10} aerosol, comparisons between measured and calculated σ_{sp} and σ_{bsp} were performed for both, the winter and summer data sets. As described in Sect. 3, σ_{sp} and σ_{bsp} were calculated based on the combined PNSD measured by TDMPs and APS. A modified Mie code was applied for simulating the measurements of Nephelometer. Calculations were carried out for the wavelengths 450, 550 and 700 nm corresponding to the wavelengths of integrating nephelometer. Based on the two-component aerosol model, either completely external or internal aerosol mixing states were assumed to derive the refraction indices.

The σ_{ap} was also calculated for 637 nm using the model, data, and mixing states mentioned above. The result was compared to the σ_{ap} measured by the MAAP. This comparison is actually not a real closure study, since the MAAP-derived BC mass concentration is also used in the model to calculate σ_{ap} .

Measured σ_{sp} (σ_{bsp}) versus calculated σ_{sp} (σ_{bsp}) at the wavelength of 550 nm and measured σ_{ap} versus calculated σ_{ap} at the wavelength of 637 nm are shown for both campaign periods in Fig. 6. In general, σ_{sp} and σ_{bsp} calculated for external mixture are slightly larger than that for internal mixture. For wavelengths of 450, 550 and 700 nm, $\sigma_{sp,external}$ are respectively factors of 1.14, 1.10 and 1.06 larger than $\sigma_{sp,internal}$, while $\sigma_{bsp,external}$ are respectively factors of 1.26, 1.19 and 1.13 larger than $\sigma_{bsp,internal}$. However, the σ_{ap} calculated for internal mixture is much larger than that for external mixture, as a factor of 2.32. This is because for external mixture, only BC particles make contribution to absorption; while for internal mixture, BC is dispersed in all particles leading to the well-known enhancement of absorption. For the same BC concentration, particles for internal mixture have larger absorbing section than for external mixture (Jacobson, 2000; Cheng, 2007).

Aerosol optical properties in the North China Plain

N. Ma et al.

Title Page

Abstract

Introduction

Conclusions

References

Tables

Figures

◀

▶

◀

▶

Back

Close

Full Screen / Esc

Printer-friendly Version

Interactive Discussion



Aerosol optical properties in the North China Plain

N. Ma et al.

Title Page

Abstract

Introduction

Conclusions

References

Tables

Figures

◀

▶

◀

▶

Back

Close

Full Screen / Esc

Printer-friendly Version

Interactive Discussion



To quantify the comparison of calculated and measured values, linear fitting was applied for σ_{sp} , σ_{bsp} and σ_{ap} . We assume that the relationship between calculated and measured values is $\sigma_{\text{model}} = b \cdot \sigma_{\text{measure}}$. Since the values spread over 3 orders of magnitudes, if the fitting was done in linear coordinates, the large values will be over-represented. Therefore, the fitting formula is modified as $\log(\sigma_{\text{model}}) = \log(b) + \log(\sigma_{\text{measure}})$ to yield more reasonable results.

Table 2 summarizes the fitting parameter b and the correlation coefficients (R) for σ_{sp} , σ_{bsp} and σ_{ap} . It can be noted that for both campaign periods, measured values and calculated values have significant correlations for the three wavelengths. At all of the three wavelengths, the correlation coefficients are above 0.98. The fitting parameters b are all around 1 for all the wavelengths.

As mentioned above, atmospheric aerosol particles are partial combinations of internal and external mixtures, due to their sources, physical and chemical processes, and stage of mixing state. The measured values should fall within the range limited by the calculated values for internal and external mixture.

It should be noticed that only a small part of the measured data is in the range of the corresponding calculated values for internal and external mixture, as shown in Table 3. The ratios of measured data that enclosed by the calculated values are low, varying from 1.6% to 84.4% for different wavelengths and parameters. Discrepancies probably stem from the uncertainties of measurements and models, which have not been taken into account. Analysis of uncertainties for dry aerosol optical closure is needed for such comparison.

4.2.2 Uncertainties of dry aerosol optical closure

To estimate the influence of the uncertainties in the model input parameters on the calculated σ_{sp} and σ_{bsp} , a Monte Carlo simulation was applied for both winter and summer datasets. The simulation repeatedly uses a set of randomly varied input parameters with normally distributed frequency.

4.3 Uncertainties of measurements

The model input parameters used in the dry aerosol closure are listed in Table 4. For each parameter, the deviation is considered to conform to a normal distribution. The original value of model input parameters mentioned in Sect. 3 is applied as the mean value. The standard deviations of normal distribution for these values are listed in Table 4.

There are many factors influencing the uncertainties in number concentration and particle size, including CPC, UCPC, APS and DMA measurement uncertainties. The TDMPs measurement induces uncertainties in size and number concentration. From a comparison test reported by Wiedensohler et al. (2011), the uncertainty of $D_{p,TDMPs}$ is estimated of 3.5%, and the uncertainties of N_{TDMPs} are estimated of 30%, 10% and 25% for size of 3–20 nm, 20–200 nm and 200–700 nm, respectively. The APS measurement induces uncertainties of 9% and 10% in size and number concentration, respectively (Wex et al., 2002a). The uncertainty in BC mass concentration measured by MAAP is estimated as 12%, as reported by Petzold et al. (2004). In open literatures, BC density is reported from 1.00 to 2.00 g cm⁻³ (Sloane et al., 1983, 1984, 1991; Sloane and Wolff, 1985; Ouimette and Flagan, 1982; Seinfeld and Pandis, 1998). The standard deviation of BC density is conformed to cover the above mentioned range. Similarly, the standard deviation for the refractive indices is also chosen to agree with the values reported in open literatures (Ouimette and Flagan, 1982; Sloane, 1984; Seinfeld and Pandis, 1998; Covert et al., 1990). The uncertainty of measured σ_{sp} and σ_{bsp} is estimated at 10% (Anderson et al., 1998; Heintzenberg et al., 2006).

4.4 Monte Carlo variations

A Monte Carlo simulation was applied to obtain the uncertainties of the results introduced by the Mie model input parameters. Mie calculation was repeated with each data record of the measurements, using a randomly varying set of input parameters. The random values of input parameters were chosen according to Table 4, and distributed

Title Page

Abstract

Introduction

Conclusions

References

Tables

Figures

◀

▶

◀

▶

Back

Close

Full Screen / Esc

Printer-friendly Version

Interactive Discussion



as normal distributions. Several hundreds of runs were done for each of the 3492 data records in winter and 3553 data records in summer to obtain the standard deviation of the σ_{sp} and σ_{bsp} at all three wavelengths, for both external and internal mixture.

Table 5 summarizes the model results of mean standard deviation of the σ_{sp} and σ_{bsp} derived from Monte Carlo simulations. It can be found that the standard deviation of calculated σ_{sp} and σ_{bsp} is around 8%. For normal distribution the range of mean value plus/minus triple standard deviation covers 99% of all possible values. Thus, the uncertainties of the Mie model results are equaled to the value of triple standard deviation. The uncertainty for calculated σ_{sp} and σ_{bsp} is approximately within $\pm 30\%$.

Comparisons similar to those described in Sect. 4.2.1 are carried out for the measured and calculated values, taking into account the uncertainties of the parameters. For the σ_{sp} and σ_{bsp} , the calculated value for external mixture plus triple standard deviation and the calculated value for internal mixture minus triple standard deviation are defined as the boundary of the possible measurement range.

Table 6 displays the ratio of measured σ_{sp} and σ_{bsp} which included in the possible range against the number of total measurements. For all the three wavelengths, more than 98% of the measured σ_{sp} falls within the possible range of Mie calculations for both winter and summer.

The results of closure for backscattering are not as good as for total scattering. The possible reason is that compared with total scattering, the backscattering is probably more sensitive to the shape of the particle. Non-spherical particles may cause higher backscattering than spherical ones. An indirect evidence is that high backscattering ratio (b) was observed during dust event in HaChi campaign. Dust has non-spherical shape and makes significant contribution to aerosol optical properties during dust event. Therefore, with the assumption of spherical shape for all particles, the Mie calculation will underestimate the backscattering.

Considering the uncertainties, most of the measured σ_{sp} and σ_{bsp} agree with the calculated values. However, the uncertainties for the calculated σ_{sp} and σ_{bsp} are approximately $\pm 30\%$. This is mainly due to the large uncertainties of the Mie model input

Aerosol optical properties in the North China Plain

N. Ma et al.

Title Page

Abstract

Introduction

Conclusions

References

Tables

Figures

◀

▶

◀

▶

Back

Close

Full Screen / Esc

Printer-friendly Version

Interactive Discussion



parameters. To reduce such uncertainties of calculation results, effort should be made to further improve measurement techniques to minimize the uncertainties of measured parameters. And more high quality measurements of aerosol chemical properties are required to reduce the uncertainties in aerosol refractive indices.

5 Summary and conclusions

In winter and summer of 2009, two field campaigns of aerosol physical properties were carried out in Wuqing, Tianjin of the NCP. In this investigation, we analyzed aerosol optical properties and conducted an optical closure experiment to examine the measurements and evaluate the uncertainties of measured parameters. The mean values of the measured σ_{sp} are 280 ± 253 and $379 \pm 251 \text{ Mm}^{-1}$ at 550 nm in winter and summer, respectively. These values are lower than those measured in urban area of Beijing (Bergin et al., 2001), similar to those measured in Yufa (Garland et al., 2009) and twice as much as that measured in SDZ (Yan et al., 2008). The mean values of the σ_{ap} during the two periods were 47 ± 38 and $43 \pm 27 \text{ Mm}^{-1}$, respectively. They are only a half of that measured in Beijing urban area (Bergin et al., 2001), slightly lower than those measured in Yufa (Garland et al., 2009) and three times as much as those measured in SDZ (Yan et al., 2008). Overall, the σ_{sp} and σ_{ap} in Wuqing were higher than those in the regional area of the NCP, while are lower than those measured in urban of Beijing. The average values of ω for dry aerosols are 0.83 ± 0.05 for winter and 0.87 ± 0.05 for summer. Three and two episodes with increased levels of pollution were observed in winter and summer campaign, respectively.

Pronounced diurnal cycle was found for different aerosol properties. The maximum value of the σ_{sp} and σ_{ap} appeared at 06:00–08:00, and began to decrease at 08:00. A minimum was reached around 16:00. During night, the σ_{sp} and σ_{ap} remained at relative high values. This diurnal pattern is mainly influenced by the diurnal variation of the boundary layer, and direct particle emissions. The ω diurnal pattern shows two dips in the morning and evening probably caused by the truck emissions. The maximum ω

Aerosol optical properties in the North China Plain

N. Ma et al.

Title Page

Abstract

Introduction

Conclusions

References

Tables

Figures

◀

▶

◀

▶

Back

Close

Full Screen / Esc

Printer-friendly Version

Interactive Discussion



occurs in the afternoon due to secondary aerosol formation and aging processes of non-absorbing aerosol particles.

Aerosol optical properties were also highly related to the meteorological parameters. The average σ_{sp} and σ_{ap} for southerly winds were higher than for northerly winds caused by the significant transport of pollutants from southern regions. In winter, the maximum σ_{sp} and σ_{ap} occurred during periods with calm winds indicating accumulation of local particle emissions. In summer, the maximum σ_{sp} and σ_{ap} occurred with southerly winds relating to the pollutants transport from southern areas. The ω accompanied by calm winds was always lower than for periods with higher wind speeds indicating a high fraction of BC in the locally emitted aerosol. The average ω for southerly winds was lower than for northerly winds, because of the higher emission rates of BC in the southern areas of the NCP.

An aerosol optical closure experiment was applied for both of winter and summer measurements. Measured σ_{sp} and σ_{bsp} was compared with the corresponding calculated values obtained via a modified Mie model. The calculation was based on measured PNSD and estimated refractive indices. A two-component aerosol model was assumed in the calculations. The σ_{sp} and σ_{bsp} were calculated separately under an assumption of internal mixture and external mixture of aerosols. Additionally, Monte Carlo simulations were used to estimate the dependence of the σ_{sp} and σ_{bsp} calculation uncertainties on the uncertainties of input parameters used in the Mie model.

Good correlations are found between measured and calculated σ_{sp} and σ_{bsp} with $R > 0.98$, confirming a stable performance of instruments. Considering the uncertainties of all input parameters used in the Mie model, Monte Carlo simulations show standard deviations of around 8% with an uncertainty within 30% for the calculated σ_{sp} and σ_{bsp} . More than 98% of measured σ_{sp} at all the three wavelengths fall within the 99% confidence range of the calculated values, taking into account of the uncertainties of measured and calculated values. The modified Mie model and corresponding assumptions used for the optical closure study are appropriate for estimating the aerosol optical properties.

Aerosol optical properties in the North China Plain

N. Ma et al.

[Title Page](#)[Abstract](#)[Introduction](#)[Conclusions](#)[References](#)[Tables](#)[Figures](#)[◀](#)[▶](#)[◀](#)[▶](#)[Back](#)[Close](#)[Full Screen / Esc](#)[Printer-friendly Version](#)[Interactive Discussion](#)

Acknowledgements. This work is supported by the National Natural Science Foundation of China (NSFC) under Grant No. 40875001 and by the German Science Foundation under grant DFG WI 1449/14-1. Funds for this experiment were also provided by: China 973 project 2011CB403402, NSFC project 40975083 and Basic Research Fund of China Academy of Meteorological Sciences 2008Z011.

References

- Anderson, T. L. and Ogren, J. A.: Determining aerosol radiative properties using the TSI 3563 Integrating Nephelometer, *Aerosol Sci. Technol.*, 29, 57–69, 1998.
- Anderson, T. L., Covert, D. S., Marshall, S. F., Laucks, M. L., Charlson, R. J., Waggoner, A. P., Ogren, J. A., Caldow, R., Holm, R. L., Quant, G., Sem, J., Wiedensohler, A., Ahlquist, N. A., and Bates, T. S.: Performance characteristics of a High-sensitivity, three-wavelength total scatter/backscatter nephelometer, *J. Atmos. Ocean. Tech.*, 13, 967 – 986, 1996.
- Albrecht, B. A.: Aerosols, cloud microphysics, and fractional cloudiness, *Science*, 245, 1227–1230, 1989.
- Bergin, M. H., Cass, G. R., Xu, J., Fang, C., Zeng, L. M., Yu, T., Salmon, L. G., Kiang, C. S., Tang, X. Y., Zhang, Y. H., and Chameides, W. L.: Aerosol radiative, physical, and chemical properties in Beijing during June 1999, *J. Geophys. Res.*, 106(D16), 17969–17980, 2001.
- Birmili, W., Stratmann, F., and Wiedensohler, A.: Design of a DMA-based size spectrometer for a large particle size range and stable operation, *J. Aerosol Sci.*, 30(4), 549–533, 1999.
- Bodhaine, B. A.: Aerosol absorption measurements at Barrow, Mauna Loa and the South Pole, *J. Geophys. Res.*, 100, 8967–8975, 1995.
- Bohren, C. F. and Huffman, D. R.: *Absorption and Scattering of Light by Small Particles*, John Wiley, Hoboken, NJ, 1983.
- Bond, T. C., Charlson, R. J., and Heintzenberg, J.: Quantifying the emission of light-absorption particles: measurements tailored to climate studies, *Geophys. Res. Lett.*, 25(3), 337–340, 1998.
- Bond, T. C., Streets, D. G., Yarber, K. F., Nelson, S. M., Woo, J.-H., and Klimont, Z.: A technology-based global inventory of black and organic carbon emissions from combustion, *J. Geophys. Res.*, 109, D14203, doi:10.1029/2003jd003697, 2004.
- Chandra, S., Satheesh, S. K., and Srinivasan, J.: Can the state of mixing of black carbon

Aerosol optical properties in the North China Plain

N. Ma et al.

Title Page

Abstract

Introduction

Conclusions

References

Tables

Figures

◀

▶

◀

▶

Back

Close

Full Screen / Esc

Printer-friendly Version

Interactive Discussion



Aerosol optical properties in the North China Plain

N. Ma et al.

[Title Page](#)[Abstract](#)[Introduction](#)[Conclusions](#)[References](#)[Tables](#)[Figures](#)[◀](#)[▶](#)[◀](#)[▶](#)[Back](#)[Close](#)[Full Screen / Esc](#)[Printer-friendly Version](#)[Interactive Discussion](#)

aerosols explain the mystery of “excess” atmospheric absorption?, *Geophys. Res. Lett.*, 31, L19109, doi:10.1029/2004GL020662, 2004.

Charlson, R. J., Schwartz, S. E., Hales, J. M., Cess, R. D., Coakley, J. A., Jr., Hansen, J. E., and Hofmann, D. J.: Climate forcing by anthropogenic aerosols, *Science*, 255, 423–430, doi:10.1126/science.255.5043.423, 1992.

Cheng, Y. F.: Aerosol radiative properties at Xinken in Pearl River Delta of China: An observation based numerical study, Ph.D. Thesis, Peking University, 2007.

Cheng, Y. F., Eichler, H., Wiedensohler, A., Heintzenberg, J., Zhang, Y. H., Hu, M., Herrmann, H., Zeng, L. M., Liu, S., Gnauk, T., Brüggemann, E., and He, L. Y.: Mixing state of elemental carbon and non-light-absorbing aerosol components derived from in situ particle optical properties at Xinken in Pearl River Delta of China, *J. Geophys. Res.*, 111, D20204, doi:10.1029/2005JD006929, 2006.

Cheng, Y. F., Wiedensohler, A., Eichler, H., Su, H., Gnauk, T., Brüggemann, E., Herrmann, H., Heintzenberg, J., Stanina, J., Tuch, T., Hu, M., and Zhang, Y. H.: Aerosol optical properties and related chemical apportionment at Xinken in Pearl River Delta of China, *Atmos. Environ.*, 42, 6351–6372, 2008a.

Cheng, Y. F., Wiedensohler, A., Eichler, H., Heintzenberg, J., Tesche, M., Ansmann, A., Wendisch, M., Su, H., Althausen, D., Herrmann, H., Gnauk, T., Brüggemann, E., Hu, M., and Zhang, Y. H.: Relative humidity dependence of aerosol optical properties and direct radiative forcing in the surface boundary layer at Xinken in Pearl River Delta of China: An observation based numerical study, *Atmos. Environ.*, 42, 6373–6397, 2008b.

Cheng, Y. F., Berghof, M., Garland, R. M., Wiedensohler, A., Wehner, B., Müller, T., Su, H., Zhang, Y. H., Achtert, P., Nowak, A., Pöschl, U., Zhu, T., Hu, M., and Zeng, L. M.: Influence of soot mixing state on aerosol light absorption and single scattering albedo during air mass aging at a polluted regional site in northeastern China, *J. Geophys. Res.*, 114, D00G10, doi:10.1029/2008JD010883, 2009.

Cooke, W. F., Lioussé, C., Cachier, H., and Feichter, J.: Construction of a 1×1 fossil fuel emission data set for carbonaceous aerosol and implementation and radiative impact in the ECHAM4 model, *J. Geophys. Res.*, 104, 22137–22162, 1999.

Covert, D. S., Heintzenberg, J., and Hansson, H. C.: Electro-optical detection of external mixtures in aerosols, *Aerosol Sci. Technol.*, 12, 446–456, 1990.

DeCarlo, P. F., Slowik, J. G., Worsnop, D. R., Davidovits, P., and Jimenez, J. L.: Particle Morphology and Density Characterization by Combined Mobility and Aerodynamic Diameter

Aerosol optical properties in the North China Plain

N. Ma et al.

[Title Page](#)[Abstract](#)[Introduction](#)[Conclusions](#)[References](#)[Tables](#)[Figures](#)[◀](#)[▶](#)[◀](#)[▶](#)[Back](#)[Close](#)[Full Screen / Esc](#)[Printer-friendly Version](#)[Interactive Discussion](#)

- Measurements. Part 1: Theory, *Aerosol Sci. Technol.*, 38(12), 1185–1205, 2004.
- Dubovik, O., Holben, B. N., Eck, T. F., Smirnov, A., Kaufman, Y. J., King, M. D., Tanre, D., and Slutsker, I.: Variability of absorption and optical properties of key aerosol types observed in worldwide locations, *J. Atmos. Sci.*, 59, 590–608, 2002.
- 5 Garland, R. M., Schmid, O., Rose, D., Nowak, A., Achtert, P., Wiedensohler, A., Gunthe, S.S., Takegawa, N., Kita, K., Kondo, Y., Hu, M., Shao, M., Zeng, L. M., Zhu, T., Andreae, M. O., and Pöschl, U.: Aerosol optical properties observed during Campaign of Air Quality Research in Beijing 2006 (CAREBeijing-2006): Characteristic differences between the inflow and outflow of Beijing city air, *J. Geophys. Res.*, 114, D00G04, doi:10.1029/2008JD010780, 2009.
- 10 Heintzenberg, J. and Charlson, R. J.: Design and applications of the integrating nephelometer: a review, *J. Atmos. Ocean. Tech.*, 13, 987–1000, 1996.
- Heintzenberg, J., Wiedensohler, A., Tuch, T. M., Covert, D. S., Sheridan, P., Ogren, J. A., Gras, J., Nessler, R., Kleefeld, C., Kalivitis, N., Aaltonen, V., Wilhelm, R. T., and Havlicek, M.: Intercomparisons and aerosol calibrations of 12 commercial integrating nephelometer of three manufacturers, *J. Atmos. Ocean. Tech.*, 23, 902–914, 2006.
- 15 Heintzenberg, J., Cheng, Y. F., and Wehner, B.: Long-term measurements of aerosol size distribution and visibility in Beijing during 2004–2007, in preparation, 2008.
- Holler, R., Ito, K., Tohno, S., and Kasahara, M.: Wavelength dependent aerosol single-scattering albedo: Measurements and model calculations for a coastal site near the Sea of Japan during ACEAsia, *J. Geophys. Res.*, 108(D23), 8648, doi:10.1029/2002JD003250, 2003.
- 20 IPCC: *Climate Change 2007 – The Physical Science Basis*, edited by: Solomon, S., Cambridge University Press, New York, 2007.
- Jacobson, M. Z.: A physically-based treatment of elemental carbon optics: Implications ofr global direct forcing of aerosols, *Geophys. Res. Lett.*, 27(2), 217–220, 2000.
- 25 Liu, P., Zhao, C., Zhang, Q., Deng, Z., Huang, M., Ma, X., and Tie, X.: Aircraft study of aerosol vertical distributions over Beijing and their optical properties, *Tellus B*, 61, 756–767, 2009.
- Lu, Z., Streets, D. G., Zhang, Q., Wang, S., Carmichael, G. R., Cheng, Y. F., Wei, C., Chin, M., Diehl, T., and Tan, Q.: Sulfur dioxide emissions in China and sulfur trends in East Asia since 2000, *Atmos. Chem. Phys.*, 10, 6311–6331, doi:10.5194/acp-10-6311-2010, 2010.
- 30 Mie, G.: Beiträge zur optic trüber Medien speziell kolloidaler Metallösungen, *Ann. Phys.*, 25, 377–445, 1908.
- Ouimette, J. R. and Flagan, R. C.: The extinction coefficient of multicomponent aerosols, *At-*

Aerosol optical properties in the North China Plain

N. Ma et al.

[Title Page](#)[Abstract](#)[Introduction](#)[Conclusions](#)[References](#)[Tables](#)[Figures](#)[◀](#)[▶](#)[◀](#)[▶](#)[Back](#)[Close](#)[Full Screen / Esc](#)[Printer-friendly Version](#)[Interactive Discussion](#)

mos. Environ., 16, 2405–2419, 1982.

Pesava, P., Horvath, H., and Kasahara, M.: A local optical closure experiment in Vienna, *Aerosol Sci.*, 32, 1249–1267, 2001.

Petzold, A. and Schönlinner, M.: Multi-angle absorption photometry a new method for the measurement of aerosol light absorption and atmospheric black carbon, *J. Aerosol Sci.*, 35, 421–441, 2004.

Quinn, P. K., Anderson, T. L., Bates, T. S., Dlugi, R., Heintzenberg, J., v. Hoyningen-Huene, W., Kulmala, M., Russell, P. B., and Swietlicki, E.: Closure in tropospheric aerosol-climate research: A review and future needs for addressing aerosol direct shortwave radiative forcing, *Phys. Atmos.*, 69(4), 547–577, 1996.

Quinn, P. K. and Coffmann, D. J.: Local closure during the first aerosol characterization experiment (ACE 1): aerosol mass concentration and scattering and backscattering coefficients, *J. Geophys. Res.*, 103(D13), 16575–16596, 1998.

Rosenfeld, D.: TRMM observed first direct evidence of smoke from forest fires inhibiting rainfall, *Geophys. Res. Lett.*, 26(20), 3105–3180, 1999.

Rosenfeld, D.: Suppression of rain and snow by urban and industrial air pollution, *Science*, 287, 1793–1796, 2000.

Seinfeld, J. and Pandis, S.: *Atmospheric chemistry and physics: from air pollution to climate change*, Wiley, Inc., New York, 1998.

Sheridan, P. J., Delene, D. J., and Ogren, J. A.: Four years of continuous surface aerosol measurements from the Department of Energy's Atmospheric Radiation Measurement Program Southern Great Plains Cloud and Radiation Testbed site, *J. Geophys. Res.*, 106(D18), 20735–20747, 2001.

Sloane, C. S.: Optical properties of aerosols – Comparison of measurements with model calculations, *Atmos. Environ.*, 17, 409–416, 1983.

Sloane, C. S.: Optical properties of aerosols of mixed composition, *Atmos. Environ.*, 18, 871–878, 1984.

Sloane, C. S. and Wolff, G. T.: Prediction of ambient light scattering using a physical model responsive to relative humidity: Validation with measurements from Detroit, *Atmos. Environ.*, 19, 669–680, 1985.

Sloane, C. S., Watson, J., Chow, J., Pritchett, L., and Richards, L. W.: Size-segregated fine particle measurements by chemical species and their impact on visibility impairment in Denver, *Atmos. Environ., Part A*, 25, 1013–1024, 1991.

Aerosol optical properties in the North China Plain

N. Ma et al.

Title Page

Abstract

Introduction

Conclusions

References

Tables

Figures

◀

▶

◀

▶

Back

Close

Full Screen / Esc

Printer-friendly Version

Interactive Discussion



- Stratmann, F. and Wiedensohler, A.: A new data inversion algorithm for DMPS-measurements, *J. Aerosol Sci.*, 27, suppl., 1, 339–340, 1996.
- Street, D. G., Gupta, S., Waldhoff, S. T., Wang, M. Q., Bond, T. C., and Bo, Y.: Black carbon emission in China, *Atmos. Environ.*, 35, 4281–4296, 2001.
- 5 Takemura, T., Nakajima, T., Dubovik, O., Holben, B. N., and Kinne, S.: Single scattering albedo and radiative forcing of various aerosol species with a global three dimensional model, *J. Climate*, 15, 333–352, 2002.
- Tuch, T. M., Haudek, A., Müller, T., Nowak, A., Wex, H., and Wiedensohler, A.: Design and performance of an automatic regenerating adsorption aerosol dryer for continuous operation at monitoring sites, *Atmos. Meas. Tech.*, 2, 417–422, doi:10.5194/amt-2-417-2009, 2009.
- 10 Twomey, S.: Pollution and the planetary albedo, *Atmos. Environ.*, 8, 1251–1256, 1974.
- van Donkelaar, A., Martin, R. V., Brauer, M., Kahn, R., Levy, R., Verduzco, C., and Villeneuve, P. J.: Global estimates of ambient fine particulate matter concentrations from satellite-based aerosol optical depth: Development and application, *Environ. Health Perspect.*, 118, 847–855, 2010.
- 15 Wex, H.: Closure and sensitivity studies on physical parameters of rural continental aerosols, Ph.D. Thesis, Leipzig University, 2002b.
- Wex, H., Neusüß, C., Wendisch, M., Stratmann, F., Koziar, C., Keil, A., Wiedensohler, A., and Ebert, M.: Particle scattering, backscattering, and absorption coefficients: An in situ closure and sensitivity study, *J. Geophys. Res.*, 107(D21), 8122, doi:10.1029/2000JD000234, 2002a.
- 20 Wiedensohler, A., Orsini, D., Covert, D. S., Coffmann, D., Cantrell, W., Havlicek, M., Brechtel, F. J., Russell, L. M., Weber, R. J., Gras, J., Hudson, J. G., and Litchy, M.: Intercomparison study of the size-dependent counting efficiency of 26 condensation particle counters, *Aerosol Sci. Technol.*, 27, 224–242, 1997.
- 25 Wiedensohler, A., Cheng, Y. F., Nowak, A., Wehner, B., Achtert, P., Berghof, M., Birmili, W., Wu, Z. J., Hu, M., Zhu, T., Takegawa, N., Kita, K., Kondo, Y., Lou, S. R., Hofzumahaus, A., Holland, F., Wahner, A., Gunthe, S. S., Rose, D., Su, H., and Pöschl, U.: Rapid aerosol particle growth and increase of cloud condensation nucleus activity by secondary aerosol formation and condensation: A case study for regional air pollution in northeastern China, *J. Geophys. Res.*, 114, D00G08, doi:10.1029/2008JD010884, 2009.
- 30 Wiedensohler, A., Birmili, W., Nowak, A., Sonntag, A., Weinhold, K., Merkel, M., Wehner, B., Tuch, T., Pfeifer, S., Fiebig, M., Fjåraa, A. M., Asmi, E., Sellegri, K., Venzac, H., Villani, P.,

Aerosol optical properties in the North China Plain

N. Ma et al.

[Title Page](#)[Abstract](#)[Introduction](#)[Conclusions](#)[References](#)[Tables](#)[Figures](#)[◀](#)[▶](#)[◀](#)[▶](#)[Back](#)[Close](#)[Full Screen / Esc](#)[Printer-friendly Version](#)[Interactive Discussion](#)

Laj, P., Aalto, P., Ogren, J. A., Swietlicki, E., Roldin, P., Williams, P., Quincey, P., Hüglin, C., Fierz-Schmidhauser, R., Gysel, M., Weingartner, E., Riccobono, F., Santos, S., Gröning, C., Faloon, K., Beddows, D., Harrison, R., Monahan, C., Jennings, S. G., O'Dowd, C. D., Mari-
5 on, A., Horn, H.-G., Keck, L., Jiang, J., Scheckman, J., McMurry, P. H., Deng, Z. Z., Zhao, C. S., Moerman, M., Henzing, B., Leeuw, G. d.: Particle Mobility Size Spectrometers: Harmonization of Technical Standards and Data Structure to Facilitate High Quality Long-term Observations of Atmospheric Particle Number Size Distributions, AMT, submitted, 2011.

Wu, Z. J., Hu, M., Liu, S., Wehner, B., Bauer, S., Maßling, A., Wiedensohler, A., Petäjä, T., Dal
10 Maso, M., and Kulmala, M.: New particle formation in Beijing, China: statistical analysis of a 1-year data set, *J. Geophys. Res.*, 112, D09209, doi:10.1029/2006JD007406, 2007.

Xu, J., Bergin, M. H., Yu, X., Liu, G., Zhao, J., Marrico, C. M., and Baumann, K.: Measurement of aerosol chemical, physical, and radiative properties in the Yangtze delta region of China, *Atmos. Environ.*, 36, 161–173, 2002.

Xu, J., Bergin, M. H., Greenwald, R., Schauer, J. J., Shafer, M. M., Jaffrezo, J. L.,
15 and Aymoz, G.: Aerosol chemical, physical, and radiative characteristics near a desert source region of northern China during ACE-Asia, *J. Geophys. Res.*, 109, D19S03, doi:10.1029/2003JD004239, 2004.

Yan, P., Tang, J., Huang, J., Mao, J. T., Zhou, X.J., Liu, Q., Wang, Z. F., and Zhou, H. G.: The measurement of aerosol optical properties at a rural site in Northern China, *Atmos. Chem. Phys.*, 8, 2229–2242, doi:10.5194/acp-8-2229-2008, 2008.

20 Zhang, Q., Streets, D. G., Carmichael, G. R., He, K. B., Huo, H., Kannari, A., Klimont, Z., Park, I. S., Reddy, S., Fu, J. S., Chen, D., Duan, L., Lei, Y., Wang, L. T., and Yao, Z. L.: Asian emissions in 2006 for the NASA INTEX-B mission, *Atmos. Chem. Phys.*, 9, 5131–5153, doi:10.5194/acp-9-5131-2009, 2009.

Aerosol optical properties in the North China Plain

N. Ma et al.

Table 1. Statistic values of aerosol optical properties measured at dry condition (RH < 30%) (4321 data points for winter campaign and 4897 data points for summer campaign).

		Means		Std		Median	
		winter	summer	winter	summer	winter	summer
σ_{sp} (Mm ⁻¹)	450 nm	363	464	319	290	280	392
	550 nm	280	379	253	251	206	314
	700 nm	191	270	175	191	137	218
σ_{bsp} (Mm ⁻¹)	450 nm	54	60	43	37	44	51
	550 nm	45	49	37	31	35	42
	700 nm	36	41	27	26	27	34
σ_{ap} (Mm ⁻¹)	637 nm	47	43	38	27	34	37
L_V (km)	550 nm	–	4.2	–	4.1	–	4.2
ω	550 nm	0.83	0.87	0.05	0.05	0.83	0.88
b (%)	550 nm	17	13	2	1	17	13
\AA	450–700 nm	1.45	1.33	0.34	0.24	1.52	1.32

[Title Page](#)
[Abstract](#)
[Introduction](#)
[Conclusions](#)
[References](#)
[Tables](#)
[Figures](#)
[Back](#)
[Close](#)
[Full Screen / Esc](#)
[Printer-friendly Version](#)
[Interactive Discussion](#)


Aerosol optical properties in the North China Plain

N. Ma et al.

Table 2. The fitting parameter (b) and correlation coefficient (R) of the linear fits for calculated and measured σ_{sp} , σ_{bsp} and σ_{ap} .

λ	winter		summer	
	external	internal	external	internal
	σ_{sp}			
450 nm	1.12 (0.987)	0.97 (0.986)	0.896 (0.989)	0.780 (0.990)
550 nm	1.13 (0.987)	1.02 (0.986)	0.913 (0.989)	0.827 (0.990)
700 nm	1.15 (0.987)	1.08 (0.987)	0.945 (0.989)	0.889 (0.990)
	σ_{bsp}			
450 nm	0.817 (0.985)	0.646 (0.982)	0.743 (0.991)	0.575 (0.988)
550 nm	0.839 (0.986)	0.706 (0.984)	0.775 (0.991)	0.642 (0.990)
700 nm	0.850 (0.987)	0.754 (0.986)	0.759 (0.988)	0.668 (0.989)
	σ_{ap}			
637 nm	0.705 (1.00)	1.63 (0.997)	0.705 (1.00)	1.71 (0.996)

Title Page

Abstract

Introduction

Conclusions

References

Tables

Figures

◀

▶

◀

▶

Back

Close

Full Screen / Esc

Printer-friendly Version

Interactive Discussion



Aerosol optical properties in the North China Plain

N. Ma et al.

Title Page

Abstract

Introduction

Conclusions

References

Tables

Figures

◀

▶

◀

▶

Back

Close

Full Screen / Esc

Printer-friendly Version

Interactive Discussion



Table 4. Uncertainties of the input parameters for the model, given in terms of one standard deviation.

Parameter	Standard deviation (%)
$D_{p,TDMPs}$	1.1
$D_{p,APS}$	3
$N_{TDMPs,3-20\text{ nm}}$	10
$N_{TDMPs,20-200\text{ nm}}$	3.3
$N_{TDMPs,200-700\text{ nm}}$	8.3
N_{APS}	3.3
BC mass concentration	4
BC density	11
n_{non}	0.5
n_{BC}	4
i_{non}	0
i_{BC}	6.6

Aerosol optical properties in the North China Plain

N. Ma et al.

Table 5. Mean standard deviations of σ_{sp} and σ_{bsp} yielding from Monte Carlo simulation.

λ	Standard deviation of σ_{sp} (%)				Standard deviation of σ_{bsp} (%)			
	winter		summer		winter		summer	
	external	internal	external	internal	external	internal	external	internal
450 nm	8.25	9.19	8.38	9.49	7.28	8.48	7.83	9.54
550 nm	8.23	8.94	8.36	9.14	7.23	8.17	7.73	8.99
700 nm	7.87	8.35	8.13	8.62	7.16	7.80	7.60	8.40

Title Page

Abstract

Introduction

Conclusions

References

Tables

Figures

◀

▶

◀

▶

Back

Close

Full Screen / Esc

Printer-friendly Version

Interactive Discussion



Aerosol optical properties in the North China Plain

N. Ma et al.

Title Page

Abstract

Introduction

Conclusions

References

Tables

Figures

◀

▶

◀

▶

Back

Close

Full Screen / Esc

Printer-friendly Version

Interactive Discussion



Table 6. Ratios of measured σ_{sp} and σ_{bsp} included by the possible range of Mie calculations.

λ	σ_{sp}		σ_{bsp}	
	winter	summer	winter	summer
450 nm	99.71%	98.57%	87.20%	61.47%
550 nm	99.57%	98.71%	88.77%	80.05%
700 nm	99.51%	98.99%	90.58%	65.10%

Aerosol optical properties in the North China Plain

N. Ma et al.

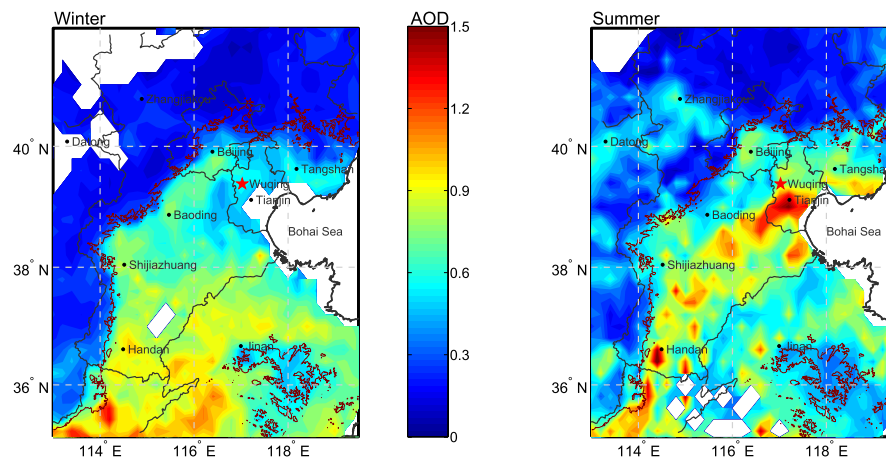


Fig. 1. The map of the NCP. The site is marked as a star. The shaded contour represents the distribution of the MODIS AOD. The dark red dashed denotes the 500 m contour line, which also can be considered as the boundary of the NCP.

Title Page

Abstract

Introduction

Conclusions

References

Tables

Figures

◀

▶

◀

▶

Back

Close

Full Screen / Esc

Printer-friendly Version

Interactive Discussion



Aerosol optical properties in the North China Plain

N. Ma et al.

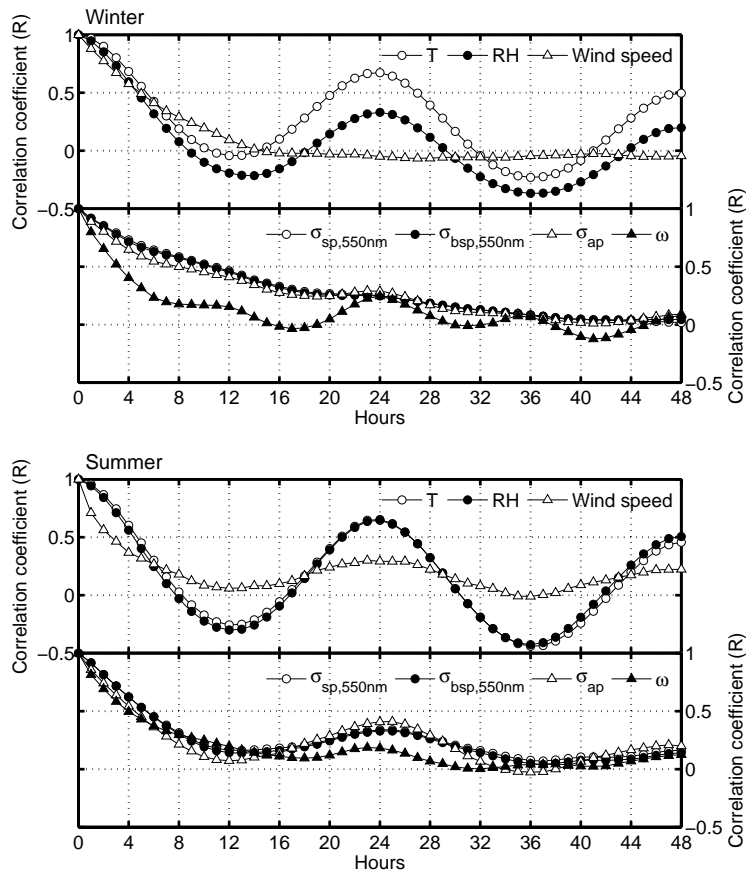


Fig. 2. Autocorrelation analysis of the meteorological parameters and the optical properties.

[Title Page](#)[Abstract](#)[Introduction](#)[Conclusions](#)[References](#)[Tables](#)[Figures](#)[◀](#)[▶](#)[◀](#)[▶](#)[Back](#)[Close](#)[Full Screen / Esc](#)[Printer-friendly Version](#)[Interactive Discussion](#)

Aerosol optical properties in the North China Plain

N. Ma et al.

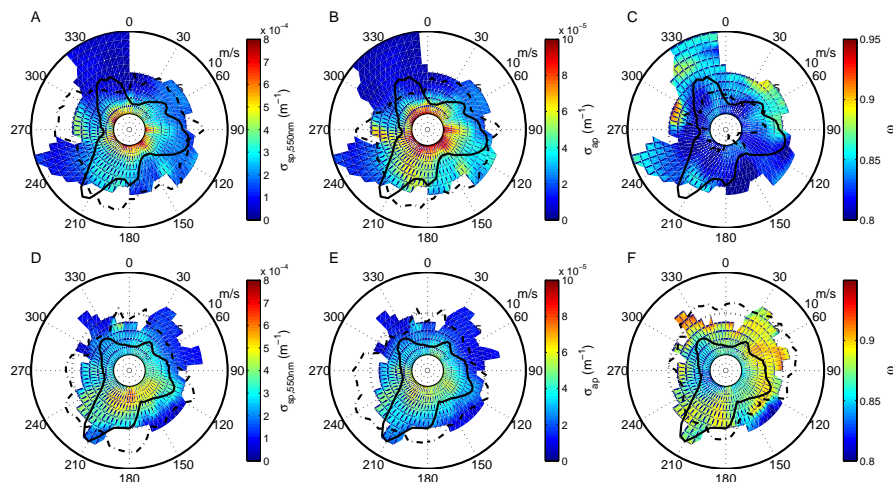


Fig. 3. Wind speed and direction dependence map of σ_{sp} (A, D), σ_{ap} (B, E) and ω (C, F). The upper three pictures are for winter and the lower ones are for summer. In each picture, the solid lines denote the wind frequency distribution. The shaded contour indicates the average of variables for varying wind speeds (radial direction) and wind directions (transverse direction). The dash-dot lines stand for average values at each wind direction.

Title Page

Abstract

Introduction

Conclusions

References

Tables

Figures

◀

▶

◀

▶

Back

Close

Full Screen / Esc

Printer-friendly Version

Interactive Discussion



Aerosol optical properties in the North China Plain

N. Ma et al.

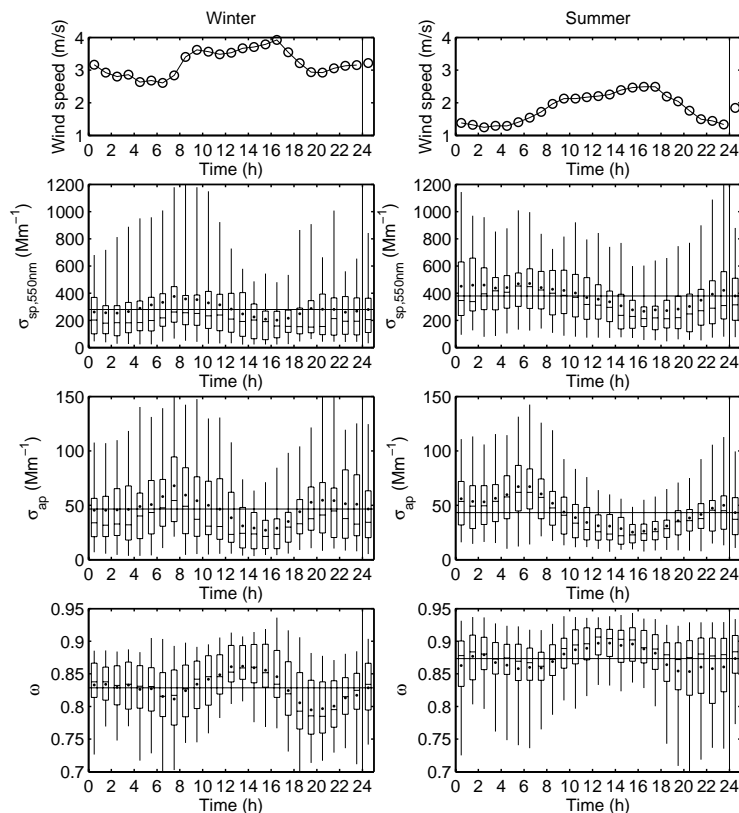


Fig. 4. Diurnal cycles of wind speed, σ_{sp} and σ_{ap} and ω . The left 4 pictures are for winter and the right ones are for summer. In each picture, the boxes and whiskers denote the 5, 25, 50, 75 and 95 percentiles, while the dots denote the mean values. The x axis denotes the time of day, with the last box-and-whisker denoting the percentile and mean value for the entire period. The horizontal line denotes the mean value for the entire study period.

Title Page

Abstract Introduction

Conclusions References

Tables Figures

◀ ▶

◀ ▶

Back Close

Full Screen / Esc

Printer-friendly Version

Interactive Discussion

Aerosol optical properties in the North China Plain

N. Ma et al.

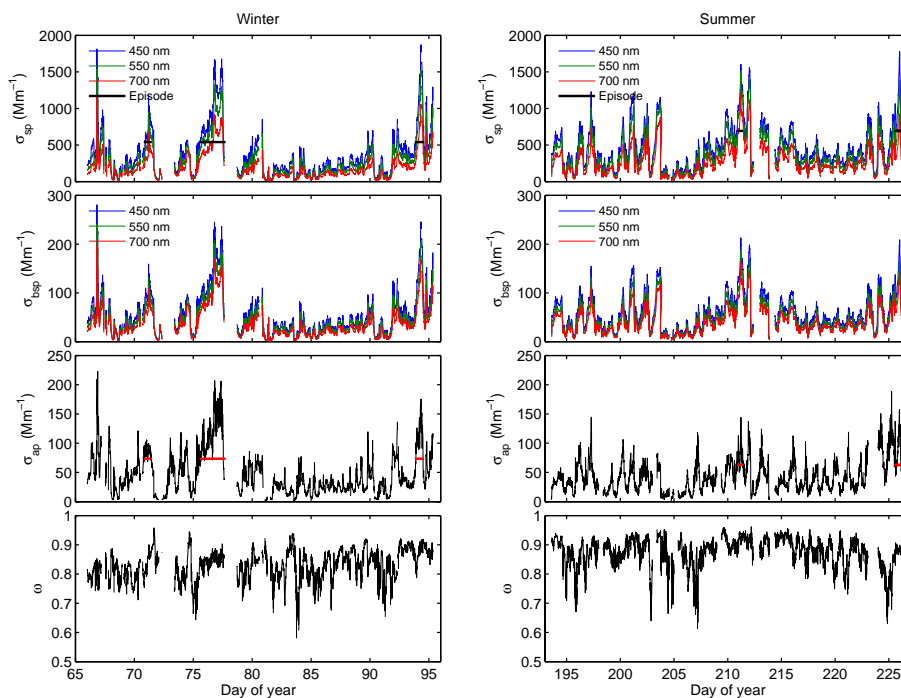


Fig. 5. Time series of measured σ_{sp} , σ_{bsp} , σ_{ap} and ω in both winter and summer campaign (RH < 30%). The horizontal short lines denote the episodes.

[Title Page](#)[Abstract](#)[Introduction](#)[Conclusions](#)[References](#)[Tables](#)[Figures](#)[◀](#)[▶](#)[◀](#)[▶](#)[Back](#)[Close](#)[Full Screen / Esc](#)[Printer-friendly Version](#)[Interactive Discussion](#)

Aerosol optical properties in the North China Plain

N. Ma et al.

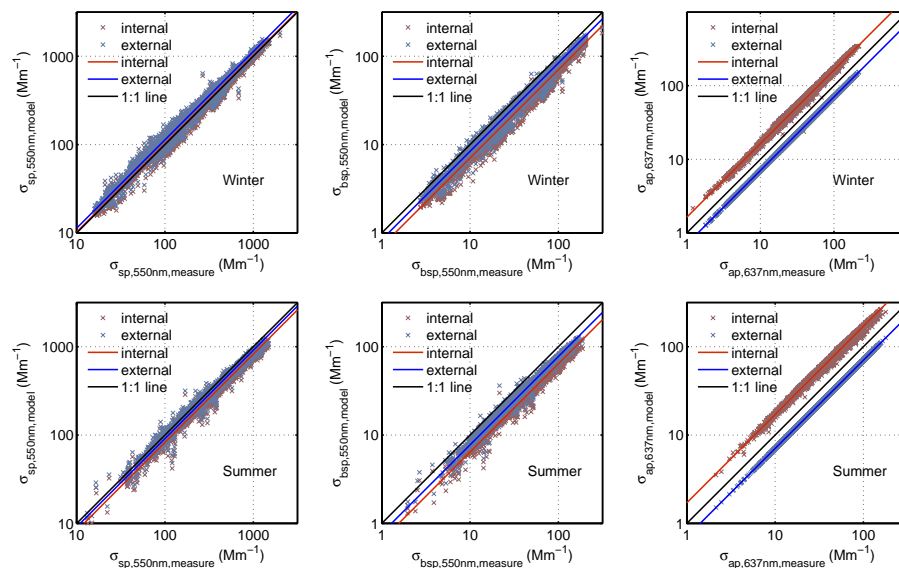


Fig. 6. Comparisons of measured and calculated σ_{sp} , σ_{bsp} and σ_{ap} in log-scale coordinates, including the 1:1 reference lines. For σ_{sp} and σ_{bsp} , only the results at 550 nm are show. The straight lines represent the linear regression fits to the data.

[Title Page](#)
[Abstract](#)
[Introduction](#)
[Conclusions](#)
[References](#)
[Tables](#)
[Figures](#)
[◀](#)
[▶](#)
[◀](#)
[▶](#)
[Back](#)
[Close](#)
[Full Screen / Esc](#)
[Printer-friendly Version](#)
[Interactive Discussion](#)
